Measurement of flow separation in a human vocal folds model

Petr Šidlof • Olivier Doaré • Olivier Cadot • Antoine Chaigne

P. Šidlof
Institute of Thermomechanics,
Academy of Sciences of the Czech Republic,
Dolejskova 5, 182 00 Prague 8, Czech
Republic e-mail: sidlof@it.cas.cz

O. Doaré · O. Cadot · A. Chaigne
Unité de Mécanique (UME), ENSTA Paris Tech,
Chemin de la Hunière, 91761 Palaiseau cedex,
France

Abstract The paper provides experimental data on flow separation from a model of the human vocal folds. Data were measured on a four times scaled physical model, where one vocal fold was fixed and the other oscillated due to fluid–structure interaction. The vocal folds were fabricated from silicone rubber and placed on elastic support in the wall of a transparent wind tunnel. A PIV system was used to visualize the flow fields immediately downstream of the glottis and to measure the velocity fields. From the visualizations, the position of the flow separation point was evaluated using a semiautomatic procedure and plotted for different airflow velocities. The separation point position was quantified relative to the orifice width separately for the left and right vocal folds to account for flow asymmetry. The results indicate that the flow separation point remains close to the narrowest cross-section during most of the vocal fold vibration cycle, but moves significantly further downstream shortly prior to and after glottal closure.

1 Introduction

Human voice is created by expiring air from the lungs through a narrow constriction called *the glottis*. This constriction is formed by the vocal folds, located in the larynx. The vocal folds (also called the vocal cords) are two symmetric soft tissue structures fixed between the thyroid cartilage and arytenoid cartilages. Basically they are composed of the thyroarytenoid muscle and ligament covered by mucosa. Under certain conditions (subglottal pressure, glottal width, longitudinal tissue tension), the vocal folds can start to oscillate and in regular phonation close the channel periodically, thus creating disturbances of the pressure field. These pressure disturbances are further filtered by the vocal tract, radiated from the mouth, and perceived as voice.

The concept of fluid–structure–acoustic interaction between the airflow, elastic vocal folds, and sub- and supraglottal acoustic spaces relies on knowledge of aerodynamics in the larynx. However, due to periodic closure of the glottal channel during vocal fold vibration and inherent unsteadiness of the airflow, the aerodynamic effects in the larynx are very complex. In spite of the progress in fundamental research of human voice production during recent years, some features of the glottal flow are not yet fully understood, one of them being flow separation from the vocal fold surfaces.

From the fluid-mechanical point of view, the human larynx can be seen as a nearly planar nozzle with time-varying clearance. In the convergent part, the airflow accelerates. Near the narrowest cross-section, airflow separates due to adverse pressure gradient and forms a jet (see Fig. 1). Although flow separation in divergent ducts has been intensively studied, usable criteria predicting flow separation are known only for simple cases. Fox and Kline (1962) published performance maps for straight and conical diffusers: in these cases, the most important factors are the area ratio, divergence angle, and inlet boundary layer blockage. Generally, the authors show that the boundary layer does not separate and the flow remains attached to

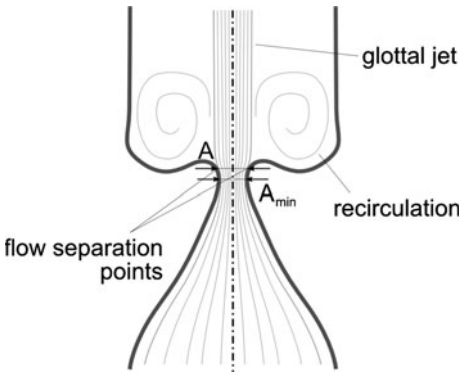


Fig. 1 Symmetric airflow in the glottis (idealization). Physiological orientation—flow in the inferior-to-superior direction

both walls only for low divergence half-angles (less than 10^o for short diffusers, less than 1^o for long ones). As the divergence angle increases, the flow shifts to transitory stall and further to bistable stall, when the flow separates from one wall only. For even higher divergence angles and diffuser lengths, there is jet flow, where the mainstream almost ignores the walls and passes at nearly constant area.

For the much more complex case of flow past human vocal folds, however, there are no general criteria predicting where exactly the flow separation takes place, as this can be influenced by many factors: interaction of the jet with supraglottal turbulent and vortical structures; flow interruption during glottal closure and formation of the new jet when the glottis reopens; whether the boundary layer has enough time to develop, etc. Yet, the information on the flow separation position is essential, e.g., in simplified computational models of phonation, where the airflow is usually modeled by Bernoulli or Euler equations. These models, still widely used due to their computational efficiency, require prior knowledge of the separation point position to obtain realistic pressure distributions along the vocal folds.

In the field of voice production research, the importance of the flow separation point movement was assessed theoretically in the paper of Krane and Wei (2006). Zhang (2008) showed in his sensitivity study that the flow separation location has significant impact on the eigenmode-coupling effect of the flow-induced stiffness, which he regards as a primary mechanism of phonation onset. He concludes that the high sensitivity to the flow separation location indicates to the need for phonation models to be capable of accurate prediction of flow separation.

In the simplified computational models of phonation, the position of the separation point is either fixed to the superior margin of the vocal folds (Story and Titze 1995; Horáček et al. 2005; Zanartu et al. 2007; Zhang et al. 2007) or supposed to move along the divergent part of the glottis. In this case, its position is usually specified using a semiempirical criterion, which states that the jet separates at the position where the channel cross-section A reaches

$$A/A_{\min} = FSC, \tag{1}$$

where $A_{\min}$ is the minimum glottal cross-section (see Fig. 1) and FSC is a constant which can be called "flow separation coefficient". In different published papers, various values of FSC are used: Deverge et al. (2003) sets $FSC = 1.2$ (based on the pioneer work of Pelorson et al. (1994) and private communication with Liljencrants), the model of Lucero (1998) assumes $FSC = 1.1$. In their comparative study, Decker and Thomson (2007) tested different values of the flow separation coefficient: $FSC = 1.2$ and $FSC = 1.47$ (according to finite volume computations of Alipour et al. (1996) and Alipour and Scherer (2004)). Recently, Cisonni et al. (2008) published data on the flow separation point coefficient computed by inverse simplified flow models. According to their results, the coefficient remains almost constant with a value $FSC = 1.08$ when a Poiseuille model is employed, or oscillates in the range $FSC = 1.02$–1.07 when a Bernoulli model is used.

It appears that a criterion for flow separation position expressed by Eq. (1) approximately holds for steady or quasi-steady flow, but its validity for intrinsically unsteady pulsating flow past vibrating vocal folds is questionable. Vilain et al. (2004) discusses this issue and proposes to solve the glottal flow alternatively by Thwaites' method within the boundary layer. This is done by Hirtum et al. (2005), whose simplified Navier–Stokes solver predicts $FSC = 1.2$–1.75.

The next controversial issue is that the criterion (1) implicitly assumes that the glottal flow is symmetric with regard to glottal mid-plane and that it separates at the same location on the right and left vocal folds. However, many of the recent works on glottal airflow dynamics, both computational and experimental, show that in reality the behavior of the glottal jet is more complex and strongly asymmetric. During vocal fold vibration, the location where the airflow separates might move down- and upstream considerably.

Hofmans et al. (2003), solving the Navier–Stokes equations by the "viscous vortex blob" method, obtained $FSC = 1.2$ for a narrow glottis and $FSC = 1.4$–1.6 for widely abducted vocal folds. The finite volume computations of Alipour and Scherer (2004) yielded $FSC = 1.1$–1.9. Thomson et al. (2005) were among the first to include fluid–structure interaction in a FEM model and compared the computational results with experiments on a true-scale rubber physical model, but did not investigate flow separation. The paper of Suh and Frankel (2007), who solved the Favre-filtered compressible Navier–Stokes equations in 3D by finite element method, was focused on flow–acoustic

interaction. Tao et al. (2007), using the Flotran solver coupled to a 2-mass model programmed in ANSYS APDL, pointed out that the asymmetry of the driving force on the vocal folds and their displacement asymmetry can reach 11%. Recently, Sciamarella and Quéré (2008) analyzed the flow past vibrating rigid vocal folds using a multigrid finite difference method and showed that the mobility of the flow separation point is nontrivial and only rarely quasi-static. The flow separation coefficient, which was evaluated, ranged between $FSC = 1.0$–1.3.

Before the laser flow measurement methods were available, the experimental papers on glottal aerodynamics, e.g., Barney et al. (1999) and Alipour and Scherer (2006), used hot-wire anemometry to measure flow velocity, or discrete pressure taps to obtain pressure distributions (Scherer et al. 2001). Neither of these methods provides sufficient spatial resolution to evaluate the position of the flow separation point. Shinwari et al. (2003), using a 7.5 times scaled plexiglass static model with vocal folds in different configurations, measured pressure distributions and obtained, among others, some quantitative data on flow separation in terms of distance from the minimal cross-section. For various transglottal pressures, the separation point was at 0.23 cm on the vocal fold, where the flow was attached, and at 0.02 cm on the opposite one.

With the development of laser flow visualization techniques and PIV, the possibilities of flow field measurements extended considerably. First, glottal flow visualizations and PIV measurements were published by Triep et al. (2005), who used a three times scaled hydrodynamic setup, and Erath and Plesniak (2006a, b) on a static 7.5 times life-size vocal fold model. Kucinschi et al. (2006) confronted his Fluent computations with pressure and flow rate measurements on a mechanically driven physical model, but did not assess velocity fields. Li et al. (2006) used a similar technique (with a static physical model) and tried to evaluate the flow separation points, although only qualitatively. Like Triep et al. (2005), Krane et al. (2007) made measurements on an externally driven model of the human glottis in a water channel, which operated at lower frequencies.

An extensive PIV data set on glottal flow was published by Neubauer et al. (2007), who used a life-sized model of Thomson et al. (2005) and quasi-phase-locked PIV to measure near-field flow structures. The paper provides detailed data on jet core velocity, jet inclination angle, and also on the flow separation point, however only qualitatively. The paper of Becker et al. (2009) is focused on elucidation of the mechanisms of sound production in the larynx. The authors used a synthetic life-sized self-oscillating vocal fold model. Their results demonstrate the existence of the Coanda effect in phonation. Erath and Plesniak (2010) published a study on asymmetric flow features in the glottis. Using an externally driven 7.5 times life-sized model precisely mimicking vocal fold oscillation, they quantify jet skewing in the divergent part of the glottis and deduce implications of flow asymmetries on sound production. In a recent paper, Triep and Brücker (2010) used an improved experimental setup equipped with time-resolved PIV to show that the supraglottal flow field is highly 3D. Their results also show that the presence of the ventricular folds decreases the pressure loss and stabilizes the jet during the divergent phase.

In spite of the considerable amount of data published on supraglottal velocity fields, there seems to be a lack of measurements with sufficient resolution to draw systematic conclusions regarding airflow separation in human phonation. This paper presents an experimental study providing quantitative data on the position of the flow separation point during vocal fold vibration. The glottal airflow in a physical self-oscillating vocal fold model was visualized using a phase-locked PIV system. The location of the flow separation point was evaluated from the visualizations by a semiautomatic procedure.

2 Methods

2.1 Vocal fold model

A new physical model of human vocal folds was designed for the current study. The model was proposed as a vocal-fold-shaped element vibrating in a rectangular channel. Unlike most of the physical models reported in previous works, in this case, the vocal fold vibration was flow-induced, not externally forced. The shape of the vocal folds that has been most widely used in mathematical and physical modeling of human voice seems to be model "M5", proposed by Scherer et al. (2001, 2002) and used, among others, in theoretical and experimental studies by him, Thomson et al. (2005), or Erath and Plesniak (2006a). The geometry of the "M5" model is piecewise linear with rounded corners. It is based on data from X-ray databases and provides an easily parametrizable approximation of the vocal fold shape during oscillation. In this work, the authors decided to specify the shape of the model vocal folds according to their own measurements of excised female human larynges in prephonatory position. The description of the methods used and a detailed quantitative specification of the vocal fold shape measured can be found in Šidlof et al. (2008). The shape was described by a piecewise cubic spline. Unlike the "M5" model, the shape is not composed of straight segments, but changes the curvature continuously. In the region where flow separation takes place (in the divergent part, downstream of the

narrowest cross-section), the radius of curvature is approximately 5.4 mm (which scales to 1.35 mm lifesize).

The model vocal folds were cast using RTV-II type 69199 two-compound silicone rubber. In the configuration presented here, the upper vocal fold was fixed to the channel wall in order to avoid asymmetric modes of vibration and situations where the vocal folds vibrate with significantly different amplitudes or even dissimilar frequencies. The second silicone vocal fold, glued on a light rigid support, was mounted on four flat springs into the wall of the channel. The prephonatory adduction of the vocal folds can be set precisely by two adjusting screws.

The physical dimensions of the real human larynx are very small, making the design of a life-sized physical model a very difficult issue. In order to perform high-resolution measurements on a mechanical model with well-defined properties, the physical model was scaled up by a factor of four. Table 1 summarizes the important dimensional and dimensionless parameters of the real larynx and the physical model, particularly the Reynolds and Strouhal numbers

$$Re = \frac{U_0 L}{\nu}, \qquad St = \frac{fL}{U_0} \tag{2}$$

based on the mean subglottal velocity U_0, kinematic viscosity ν, fundamental frequency of vibration f and vocal fold thickness L (see Fig. 2).

The elasticity of the vocal folds is modeled mainly by the stiffness of the flat springs. As shown in Fig. 4, each spring was clamped to a rigid beam on one side and screwed to the rigid support of the vocal fold on the other. The dimensions (85 × 10 × 0.5 mm) and material (brass alloy, Young modulus 100 GPa) of the springs were designed so that the first natural frequency of the system matched the desired scaled frequency. After fabrication, the force-deflection curve of the springs was measured. Within the operational limits, the response was roughly linear (slightly hardening under heavier loads), with stiffness about 200 N/m per one spring. The stiffness of the silicone rubber itself would be too large to allow self-sustained oscillation with the desired frequency and plays important role during vocal fold collisions only.

Table 1 Comparison of the relevant dimensional and dimensionless parameters: mean subglottal velocity U_0, channel height H_0, vocal fold thickness L, oscillation/vortex shedding frequency f, transglottal pressure Δp, Reynolds and Strouhal number Re and St

	Real larynx	Physical model
U_0 (m/s)	1–10	1.4–2.5
H_0 (mm)	10–20	40
L (mm)	10	40
f (Hz)	100–400	10–14
Δp (Pa)	200–2,000	50–250
Re	600–6,000	3,000–6,000
St	0.1–1	0.2–0.3

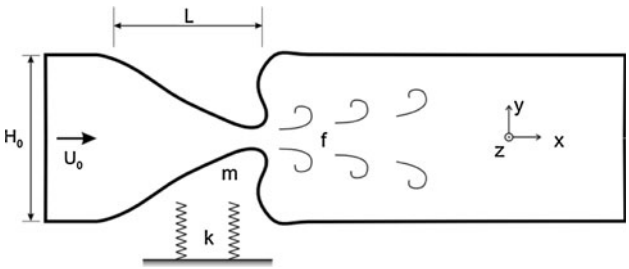


Fig. 2 Overview of the important dimensional parameters: channel height H_0, inlet flow velocity U_0, characteristic length (vocal fold thickness) L and frequency f, mass m and stiffness k

The elastic support gives the vocal fold three degrees of freedom. The first is the "heaving" (10) mode of vibration, where the vocal fold translates along the y-axis (see Fig. 2 for orientation of the coordinate system). In the second, "rocking" (11) mode, the mass rotates about the z-axis. The elastic support itself does not block the third, undesired, "torsional" (20) mode, where the vocal fold rotates about the x-axis. Frequency analysis of the impulse response shows that the natural frequency of the largely dominant heaving mode is 11.0 Hz. The second highest peak in the spectrum (about 20 dB lower than the first one) at 21.9 Hz belongs to the torsional mode. The high-speed camera recordings of flow-induced vibration revealed, however, that the torsional mode is suppressed by collisions against the opposite vocal fold and most likely also by the aerodynamic damping, since this mode did not occur even for vibration without collisions at low flow rates. The rocking mode manifests as an indistinct peak at 38 Hz. As a result, the flow-induced vibration occurs slightly above the first natural frequency and has mostly the character of the first (10) mode.

2.2 Experimental setup

The vocal fold model was mounted in a plexiglass wind tunnel. A centrifugal fan regulated by a frequency inverter drives the flow through a honeycomb screen into a long circular channel intended to suppress the inlet turbulence (see Figs. 3, 4). Further, the channel cross-section contracts smoothly by factor $f \approx 6$ into a rectangular 100 × 40 mm inlet of the measuring section with the vocal folds. Downstream of the vocal folds, the channel continues 40 cm to simulate the vocal tract and terminates freely into ambient air.

To allow free motion of the vocal fold, there has to be a small gap between the vocal fold and the channel walls. The leakage flow at the inferior margin (left edge in Fig. 3)

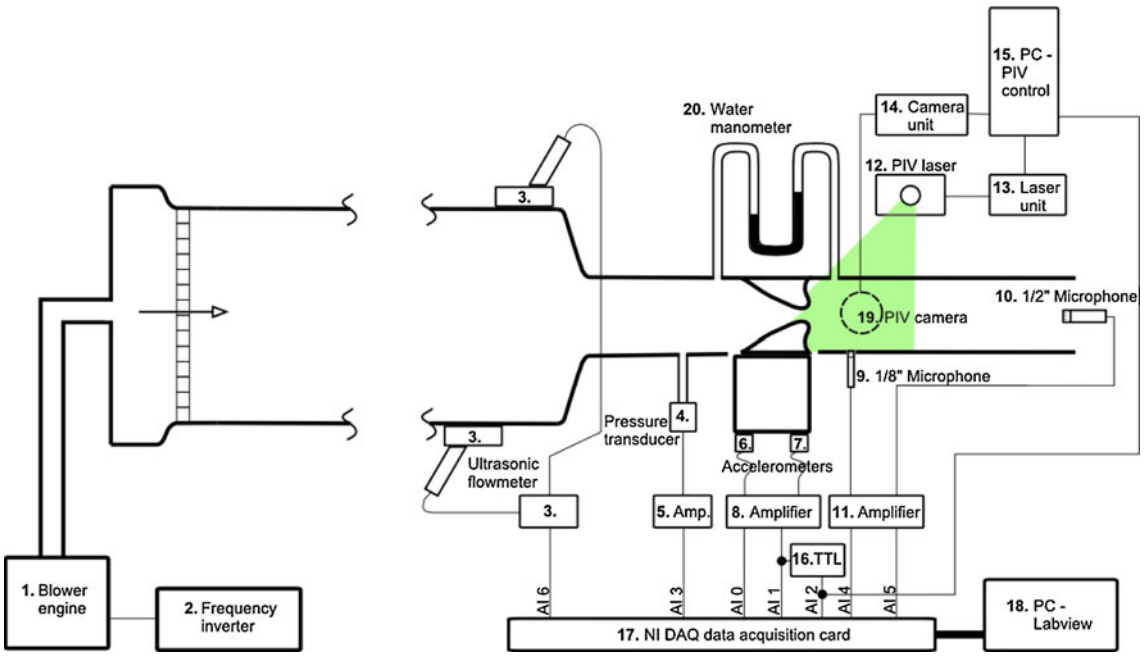


Fig. 3 Diagram of the experimental setup used for the measurements of vocal fold vibration and for visualization of the supraglottal flow. *1* Rietschle Thomas centrifugal fan (2,200 W, $\Delta p_{max} = 29\,\text{mbar}$, $Q_{max} = 2,770\,\text{m}^3/\text{h}$). *2* Omron Sysdrive 3G3MV frequency inverter (380 V, 0–60 Hz). *3* GE Panametric GC 868 ultrasonic gas flowmeter. *4* Validyne DP15TL dynamic pressure transducer (steel membrane 0.125 PSI FS). *5* Validyne CD23 amplifier. *6, 7* Brüel&Kjær 4507C accelerometers. *8* Brüel&Kjær Nexus conditioning amplifier type 2692 (frequency bandpass 1 Hz–1 kHz). *9* G.R.A.S. 1/8″ condenser microphone type 4138, G.R.A.S. preamplifier type 26AJ. *10* G.R.A.S. 1/2″ prepolarized free field microphone type 40BE, G.R.A.S. preamplifier type 26AJ. *11* Brüel&Kjær Nexus conditioning amplifier type 2690. *12* New Wave Research PIV laser SOLO 3–15. *13* New Wave Research SOLO III laser unit. *14* LaVision Imager PRO camera unit. *15* PC-2proc Intel Xeon, software Davis v7. *16* Philips PM5715 TTL/pulse generator. *17* National Instruments NI DAQPad-6015 data acquisition card. *18* PC-software NI LabView v7.1. *19* LaVision Imager PRO camera (1,600 × 1,200 pixel, Canon macro TV zoom lens). *20* Kimo water manometer (precision 0.5 mm H_2O (5 Pa))

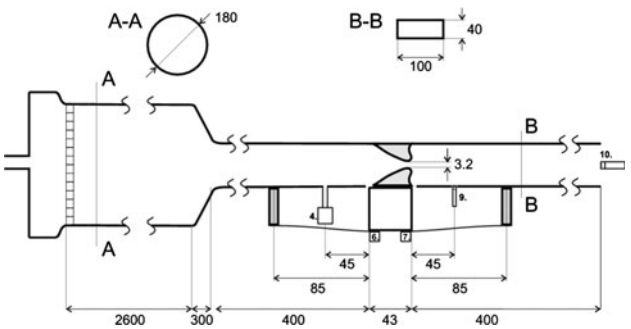


Fig. 4 Schematic of the vocal fold model and important dimensions of the wind tunnel (in millimeters)

was blocked by a thin membrane. Since the mean supraglottal pressure in the model was close to atmospheric pressure, the leakage at the superior margin was not important. The airflow along the side walls, which could not be completely avoided, did not significantly influence the supraglottal velocity fields measured in the channel mid-plane.

The setup was equipped with accelerometers (Brüel& Kjær 4507C), mounted below the apex and leading edge of the vocal fold to record vocal fold vibration. The frequency spectra of the acceleration signal were used to detect the frequency of vibration of the vocal fold. To capture the subglottal pressure including the DC part of the signal, dynamic pressure transducers (Validyne DP15TL, steel membrane 0.125 PSI FS) were used. Two microphones (G.R.A.S. 1/8” condenser microphone type 4138 mounted flush with the wall, G.R.A.S. 1/2” prepolarized free field microphone type 40BE located at the channel exit) recorded the supraglottal dynamic pressure and the radiated acoustic pressure. To measure the mean flow in the channel, an ultrasonic gas flowmeter (GE Panametric GC 868) was fixed near the downstream end of the circular channel. The diagram in Fig. 3 shows the locations and wiring of transducers used. The important dimensions are summarized in Fig. 4.

The PIV system consisted of a Nd:YAG laser (New Wave Research Solo III, maximum repetition rate 15 Hz, 120 mJ), laser unit, and the PIV camera and unit (La Vision Imager PRO, 1,600 × 1,200 pix, max. 15 frames/s). The flow was seeded from an olive oil atomizer upstream of the honeycomb screen. The camera lens (Canon macro TV zoom), fixed 1.5 cm from the plexiglass wall, had a field of view of about 60 × 45 mm, providing spatial

resolution of the raw camera frames of 0.037 mm/pix. The PIV settings were as follows: delay between pulses 20 μs, interrogation area 32 × 32 pix, 50% overlap. In order to remove the laser sheet reflections on the vocal fold surface, the raw images were preprocessed using sliding background image subtraction. The postprocessing options consisted of multi-pass correlation, peak validation, median filtering and smoothing.

The laser and camera were triggered by a rectified signal from one of the accelerometers. Hence, the system was phase-locked with the vocal fold vibration to measure the velocity fields at precisely defined phases of the oscillation cycle. Due to the low repetition frequency of the laser system (15 Hz), only one pulse could be generated per one oscillation cycle. The phase difference between the laser and vocal fold oscillation was set in such a way that during 40 subsequent periods of vibration, 40 camera frames were recorded, covering the whole oscillation cycle. The setup of the optics allowed recording the 2D flow field immediately downstream of the glottis. Due to oil particle deposition on the walls, frequent cleaning was necessary between experimental runs to preserve sufficient image sharpness.

2.3 Determination of the flow separation point from the recorded camera frames

Traditionally, the term "flow separation point" used in simplified models of glottal flow assumes that the glottal flow is symmetric with regard to the glottis midline, as depicted in Fig. 1. In this case, it is sufficient to quantify the separation point position by the glottal area at the critical place. However, flow visualizations and PIV measurements on physical models, as well as computational flow simulations based on finite element or finite volume codes, show that this is rarely the case: the glottal jet tends to attach to one of the vocal fold surfaces and significantly skews from the glottis midline position (see Fig. 5 for a schematic representation of the flow pattern).

Such asymmetric flow was observed in measurements presented in this paper, too. Therefore, it was necessary to introduce a suitable coordinate system to describe the position of the "left" and "right" separation point independently, still allowing to correlate the new results to previously used criteria for flow separation.

First, the narrowest cross-section was located (defined by the left and right VF apex in Fig. 6). The line is not necessarily perpendicular to the channel, because during vibration the apex of the vocal fold moves slightly in the horizontal direction (that is, in the inferior–superior direction in physiological orientation). Then, the "left" and "right" flow separation coefficients FSC_L and FSC_R can be defined simply as the distance of the respective flow separation point from the axis divided by half of the orifice width:

$$FSC_L = \frac{w_L}{d/2}, \quad FSC_R = \frac{w_R}{d/2}. \tag{3}$$

Such a description is a generalization of the symmetrical definition (1). If the vocal fold vibration and supraglottal velocity field were perfectly symmetrical with regard to the glottal axis, the definitions would be equivalent.

In principle, the position of the flow separation point may be evaluated from the vector fields calculated by the PIV method. However, in the PIV velocity field, a single vector is computed typically from a 32 × 32 pixel "interrogation" area, which means that the resolution of the vector field is much lower than the resolution of the original image. Moreover, the vector represents a statistical mean of particle velocities within the interrogation area.

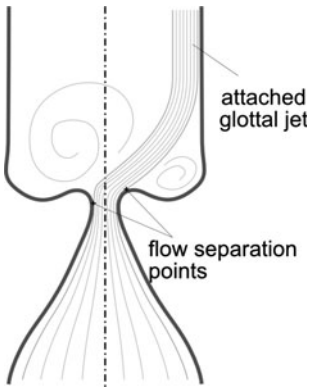


Fig. 5 Asymmetric flow in the glottis. Physiological orientation—flow in the inferior-to-superior direction

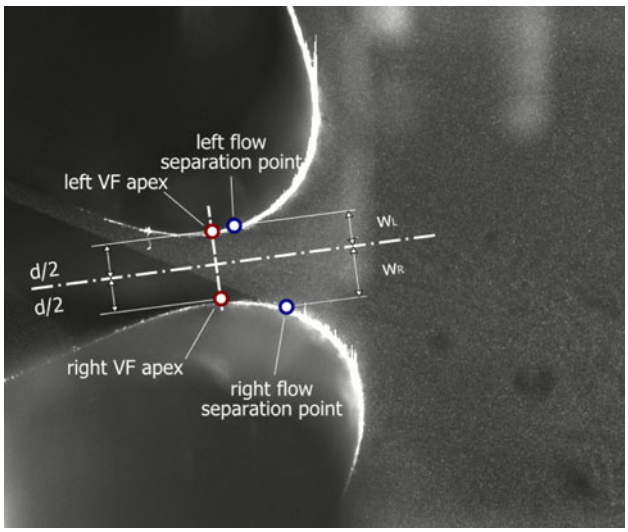


Fig. 6 Definition of the flow separation coefficient. Experimental configuration—flow direction from the *left* to the *right*

Consequently, the vector fields tend to smooth out small-scale turbulent effects and large velocity gradients.

However, when the optical setup is properly focused and the glottal area well illuminated by the laser sheet, it is possible to exploit directly the raw camera double-frames, which provide more detailed information on the small-scale flow features, although not quantitative. When the two camera frames are played consecutively in image analysis software, the boundary between the fast moving particles within the glottal jet and almost immobile particles in the supraglottal area becomes clearly evident. Figure 7 shows the raw camera frame and the computed PIV velocity field. The still figure cannot display the motion of the particles used to locate the separation points, but provides a basic insight into what flow scales are lost in the PIV field. Using this technique, it is possible to discern the glottal jet contour and the position of the flow separation point with an accuracy on the order of 0.1 mm. Even when taking into account the possible error introduced by the partly subjective character of the method, the uncertainty of the position of the flow separation point is well below 0.5 mm (0.12 mm lifesize). In the rare cases where the glottal jet was not clearly recognizable, the position of the separation point was not recorded and the value was rejected.

Technically, the evaluation procedure of the flow separation point was as follows (performed using high-speed camera image analysis software Olympus i-SPEED 2):

- the images were calibrated using the known height of the channel
- for each phase of the vocal fold oscillation, the position of the "left" and "right" flow separation point and of the vocal fold apex was located manually,
- the coordinates of the four points were recorded by the software and the left and right flow separation coefficients were calculated automatically according to Eq. (3).

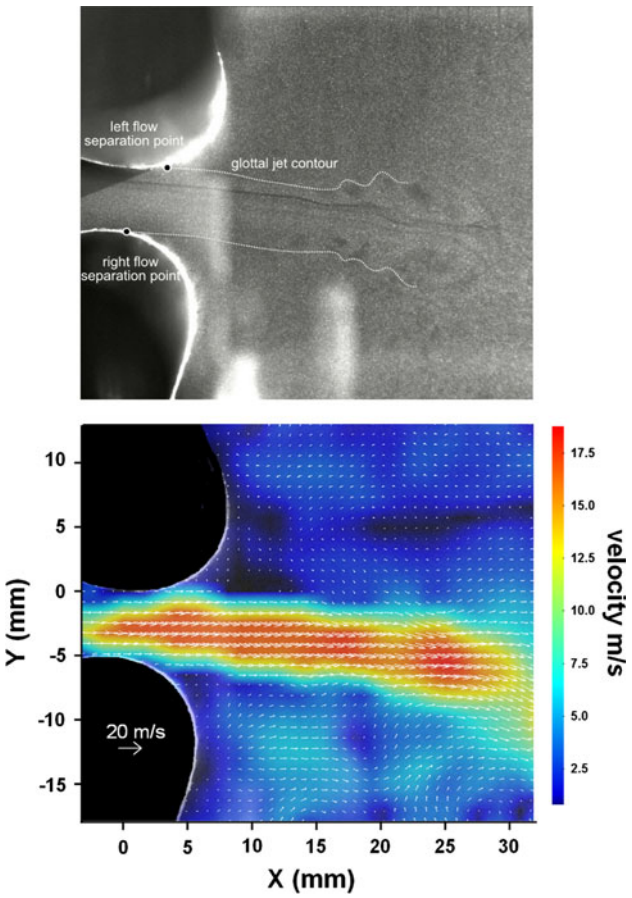


Fig. 7 Raw image recorded by the PIV camera (first frame of the double-frame) showing the positions of seeding particles (*top*). When played consecutively with the second frame, the glottal jet contours and the position where the jet separates from the vocal fold surface are clearly visible. Instantaneous vector velocity field computed by PIV (*bottom*). Measurement 012 (Re = 5,400), regular vocal fold vibration with a collision in each cycle. Frequency of vibration 13.2 Hz

3 Results

3.1 Dynamic and acoustic measurements

Although it was not the primary objective of this study to measure the dynamic response of the structure to flow excitation and the sound signal, these results help understand the dynamic and acoustic properties of the system. The vibration of the vocal fold is shown in Fig. 8. The figure depicts nine phases of an oscillation cycle from measurement 012, a case of regular vocal fold vibration with a collision in each cycle. The third phase (top right) is in the maximum glottis opening. The eighth phase (bottom, in the middle) was taken in the middle of the of the contact period, where the vocal folds approached most. This phase also reveals the maximum deformation of the vocal folds.

Figures 9 and 10 show the waveforms and spectra of the vocal fold acceleration, subglottal pressure, supraglottal pressure, and radiated acoustic pressure. The mechanical vibration for the lower flow rate (Fig. 9) is nearly sinusoidal. The non-harmonic spectral frequency of 78.5 Hz, significant also in the spectrum of the subglottal pressure, corresponds probably to subglottal acoustic resonance. In the waveforms of the microphone signals, strong broadband noise is present, caused by turbulence in the supraglottal region.

The accelerometer waveform for $Re = 5{,}400$ (Fig. 10) clearly shows the vocal fold collisions, which are visible as peaks on the positive half-waves. The acoustic signals are well correlated with the vocal fold motion and have a

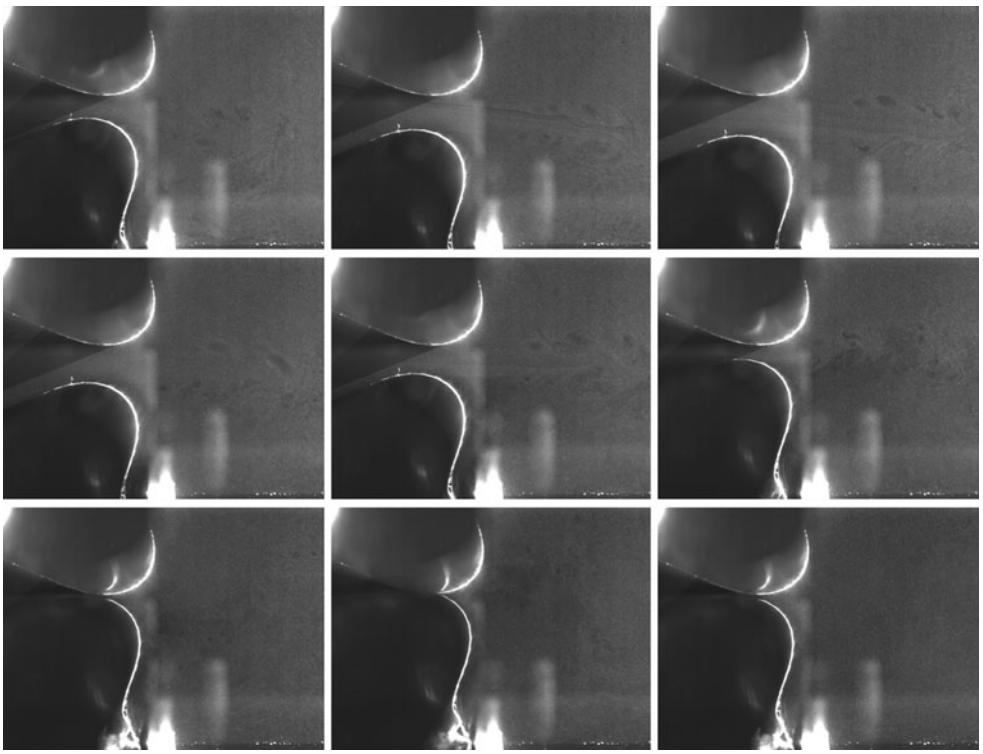


Fig. 8 Flow-induced vibration of the vocal fold—nine phases of an oscillation cycle. Measurement 012 ($Re = 5{,}400$), regular vocal fold vibration with a collision in each cycle. Frequency of vibration 13.2 Hz

periodic structure with harmonic frequencies in their spectra. The subglottal pressure appears to include less noise, but this is probably caused by the fact that unlike measuring microphones, the dynamic pressure transducer used was unable to capture high-frequency components. It is apparent that in the configuration used, the best signal to trigger the PIV system is the acceleration, which has best periodicity and signal-to-noise ratio.

3.2 Flow visualizations and PIV measurements

Figure 11 shows a typical velocity field downstream of the glottis evaluated by the PIV method. The vocal folds in the left part of the figure were masked out to show better their contours and to remove meaningless vectors. The vector plot reveals the glottal jet, which separates from the vocal fold surfaces and enters into the supraglottal domain. The jet is skewed to the right in this particular case. This tendency was observed throughout all the measurement sets, supporting the assumption that the Coanda effect is present in human phonation. In some of the measurements, the direction of the jet axis switched occasionally. However, the jet skewed preferentially to the right as in this case, probably due to slight asymmetry in the geometry of the left and right vocal folds, and possibly also due to the fact that the left (upper) vocal fold was fixed, while the right (bottom) one vibrated. In the region between the right vocal fold surface and the jet, a large recirculation vortex can be seen.

The flow visualizations (accompanied by acoustic and dynamic measurements) were performed systematically for increasing flow rates. These ranged from the lowest possible airflow able to induce self-sustained vocal fold oscillations up to the highest values realistic in human phonation.

3.3 Position of the flow separation point

The essence of this work is quantification of the flow separation point locations during vocal fold vibration, as explained in Sect. 2.3. During phonation, the glottal velocity field is not perfectly periodic and the location of the flow separation point in a specific phase can vary over subsequent cycles of vibration. Due to the highly arduous procedure of evaluation of the separation point, it is impossible to provide proper statistical information. However, it is important to asses the fluctuation of the flow separation point position at least in one case. For this purpose, four measurements recorded at identical conditions (Reynolds number $Re = 5{,}400$, vocal fold vibrations with collisions) were analyzed. In order to superimpose the results of these measurements, where the frequency of

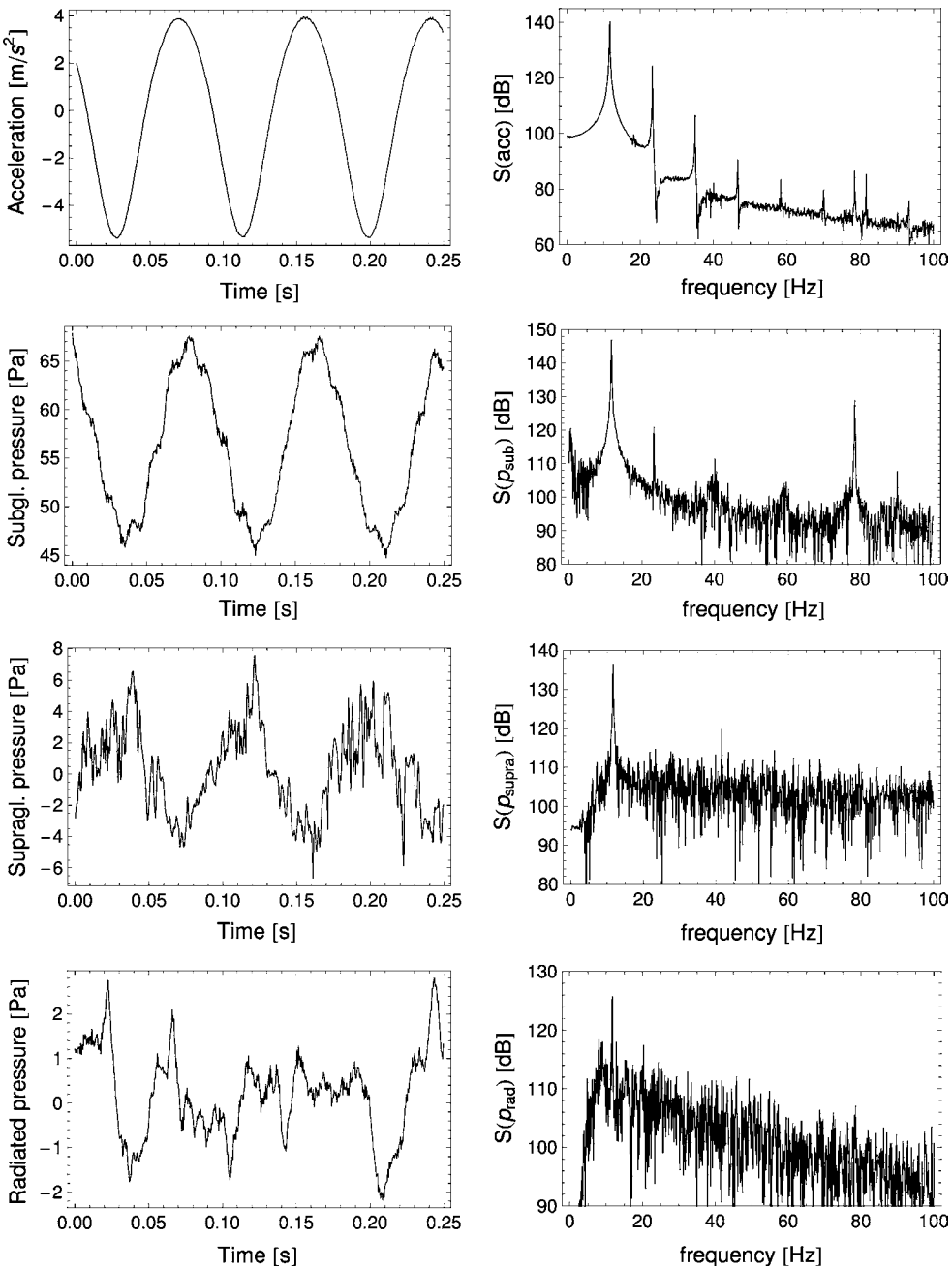


Fig. 9 Waveforms (*left*) and frequency spectra (*right*) of the acceleration, subglottal pressure, supraglottal pressure and pressure radiated at the channel exit. Measurement 002 ($Re = 3{,}500$), vocal fold vibration without a collisions. Frequency of vibration 11.7 Hz

vibration varied slightly (<0.1 Hz) and the double-frames were not taken in exactly identical phases, it was necessary to extract in each case precisely one period, align the four measurements, interpolate and resample the data.

The results in Fig. 12 show that during most of the vibration cycle, the flow separation coefficients have low variation. Near glottal closure, the data are much more scattered. This is caused by the fact that when the vocal folds collide and the jet is interrupted, the flow is highly nonstationary and the decaying or evolving jet is more susceptible to interactions with turbulent structures. In certain measurements, it was even observed that the jet changes direction over subsequent cycles and attaches to the left or right vocal fold in a random way.

In the following, the results of flow separation point measurements for three flow rates are presented. Figure 13 summarizes the results for $Re = 3{,}500$, flow rate $Q = 5.5$ L/s, transglottal pressure difference $\Delta p = 45$ Pa, frequency of vibration $f = 10.9$ Hz (corresponding to $Q = 1.4$ L/s, $\Delta p = 720$ Pa and $f = 173$ Hz lifesize). As can be seen from the orifice width plot in the right, in this case, the vocal folds did not collide throughout the oscillation cycle. Such vocal fold vibration can be observed in certain types of breathy phonation.

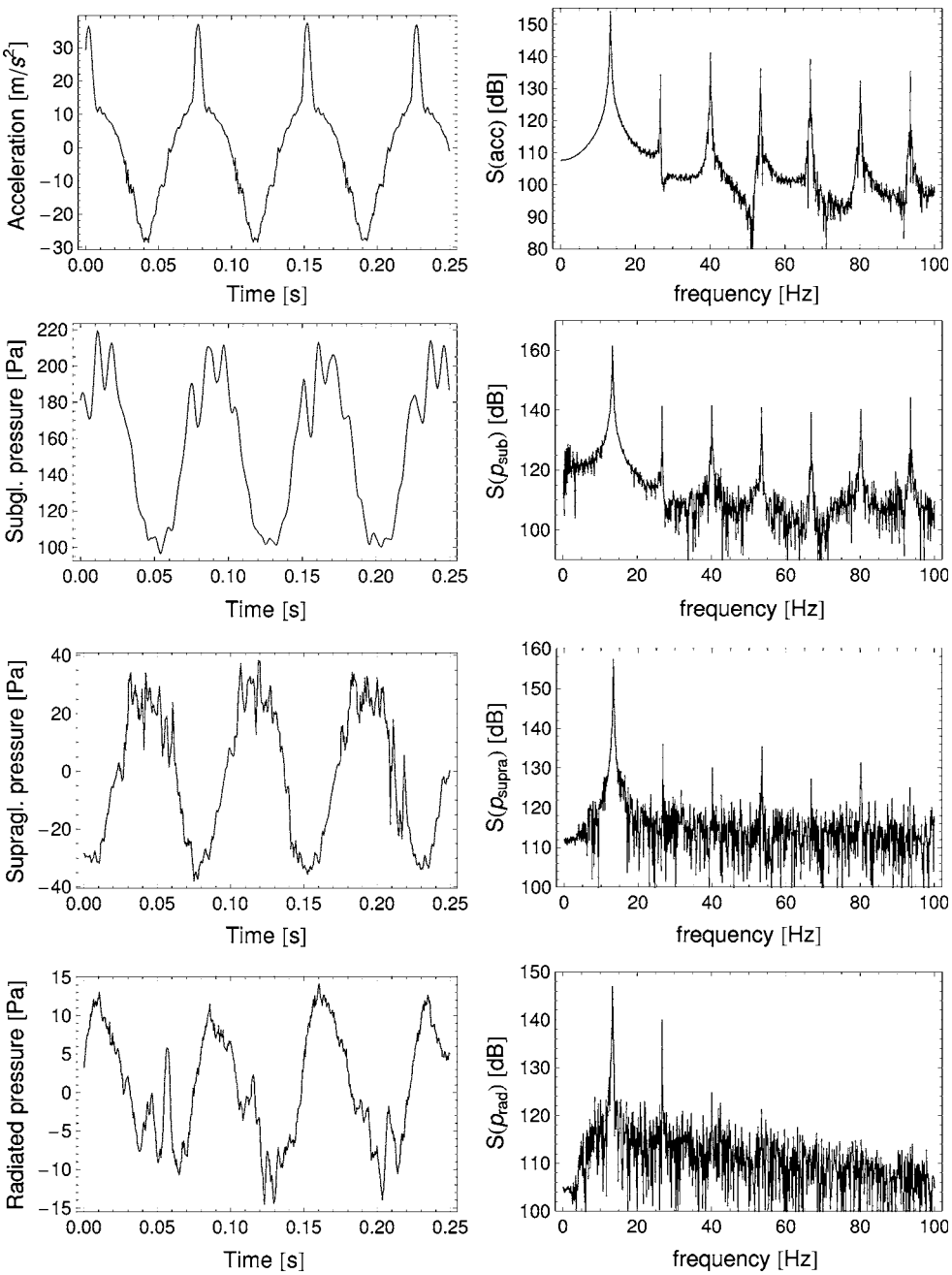


Fig. 10 Waveforms (*left*) and frequency spectra (*right*) of the acceleration, subglottal pressure, supraglottal pressure and pressure radiated at the channel exit. Measurement 012 ($Re = 5{,}400$), regular vocal fold vibration with a collision in each cycle. Frequency of vibration 13.2 Hz

Figure 13 also shows the development of the left and right flow separation coefficients during 40 phases of the vocal fold oscillation cycle. The opening and closing phases are separated by dashed lines. The vocal folds approximate the most between frames #5–7, where the opening phase begins (see the orifice width plot in Fig. 13). In a large part of the oscillation period, both left and right flow separation coefficients stay between 1.0 and 1.5. Near glottal closure and reopening, however, the FSC_R sharply increases up to about 5.5. This is a quantification of an effect, which can be seen almost universally in all measurements—when the glottal gap gets very narrow, the jet weakens and tends to attach to one of the vocal fold surfaces (in this case, the right one). Since the airflow separates very far from the narrowest cross-section, the separation coefficients reach much higher values than usually assumed.

The effect is even more prominent in cases where the vocal folds collide and the glottal gap closes. Figure 14 shows the flow separation coefficients and orifice width for $Re = 5,400, Q = 8.58\,\text{L/s}, \Delta p = 150\,\text{Pa}$ and $f = 13.4\,\text{Hz}$ (which correspond to $Q = 2.1\,\text{L/s}, \Delta p = 2,400\,\text{Pa}$ and $f = 214\,\text{Hz}$ lifesize). Again, when the glottis is wide open, the flow separation coefficient is close to 1.1, increases to

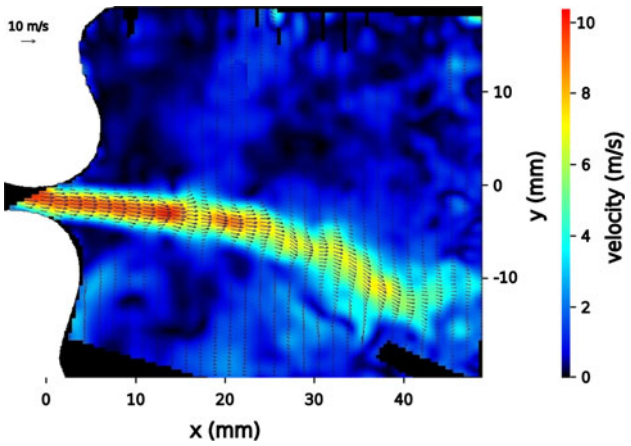


Fig. 11 Typical instantaneous flow velocity field downstream of the glottis. Measurement 002d ($Re = 3{,}500$, without glottal closure), middle of the closing phase

about 1.5 in the middle of the opening/closing phases, and sharply rises up to 20 near vocal fold contact. The jet was attached mostly to the right vocal fold, but the left separation coefficient near the glottis opening increased up to values around 5, as in previous cases. Figure 15 proves that the increase in the FSC near glottal closure is not caused by the fact, that the glottal gap d (denominator in equation 3) is small: the distance of the flow separation point from the vocal fold apex itself increases, too. This shows that the airflow separates further downstream, than when the glottis is wide open.

For the case shown in Fig. 16 ($Re = 6,600$, $Q = 10.4\,\mathrm{L/s}, \Delta p = 230\,\mathrm{Pa}, f = 13.8\,\mathrm{Hz}$, corresponding to $Q = 2.6\,\mathrm{L/s}, \Delta p = 3,600\,\mathrm{Pa}$ and $f = 220\,\mathrm{Hz}$ lifesize), FSC_R has a plateau at 1.12 and shortly before glottal closure sharply rises up to 20. The FSC_L data are more scattered, but show similar behavior.

The physical model vibrated well for a broad range of higher airflow velocities, also. The quantified data on flow separation showed very similar behavior even for these high velocities. Nevertheless, since these flow rates are beyond the physiologically relevant limits, the results are not shown here.

4 Discussion and conclusions

The main objective of this paper was to provide experimental quantitative data on glottal aerodynamics and namely on the position of the flow separation point during phonation. A physical, four times scaled vocal fold model was designed to perform the measurements. The geometry of the vocal folds was based on measurement of excised human larynges in phonation position and is slightly different from the "M5" approximation commonly used in modeling studies.

The authors believe that in order to get representative experimental data on the aerodynamics of human phonation using physical models, it is desirable that the model be self-oscillating, rather than externally driven. However, the requirement of a self-excited system brings numerous complications and technical limitations. First of all, the physical model does not provide enough free parameters (e.g., the subglottal velocity U_0) to be set independently, and thus, it cannot be ensured that the dynamic similarity of the model and the real larynx is perfect. In current measurements, nevertheless, the pertinent Reynolds and Strouhal numbers lie within the bounds encountered in human phonation.

From the same reason, the flow-induced vibration of the vocal fold model is not precisely identical with that found in the real larynx. The convergent–divergent shaping of the glottis is not mimicked by the model to the extent that can be reached in externally driven models: the current model vibrates dominantly in the 10 mode and it mostly resembles the "convergent" M5 geometry. Therefore, the results are relevant e.g., for glottal opening or for situations close to breathy voice, where the subglottal pressure is not high, prephonatory glottal diameter nonzero and where there is strong reason to believe that the glottal shape changes from divergent to convergent shortly before closing. However, considering that the shape of the medial surface of the real vocal folds during vibrations can be more complex (not strictly straight convergent or straight divergent as in the M5 model), the authors assume that the results on flow

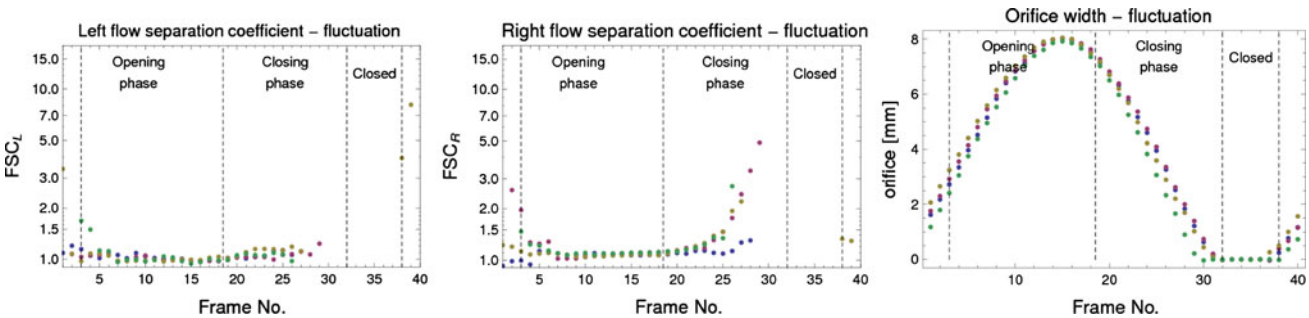


Fig. 12 Fluctuation of the *left* and *right* flow separation coefficients and of the orifice width. Measurements 012s-w ($Re = 5{,}400$, with glottal closure). *Dashed lines* delimit the boundaries of vocal fold vibration phases (*opening phase*, *closing* and *closed phase*)

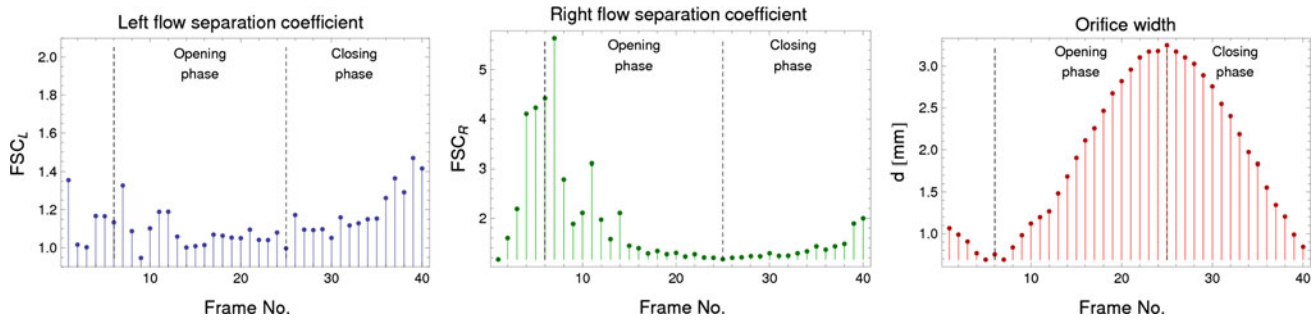


Fig. 13 Measurement 002c ($Re = 3{,}500$, without glottal closure), one oscillation cycle. *Left* and *right* flow separation coefficient, orifice width

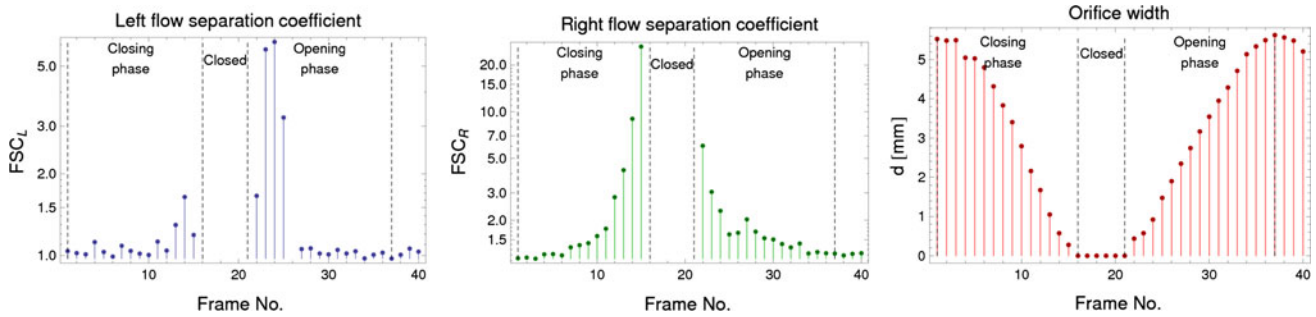


Fig. 14 Measurement 012v ($Re = 5{,}400$, with glottal closure), one oscillation cycle. *Left* and *right* flow separation coefficient, orifice width

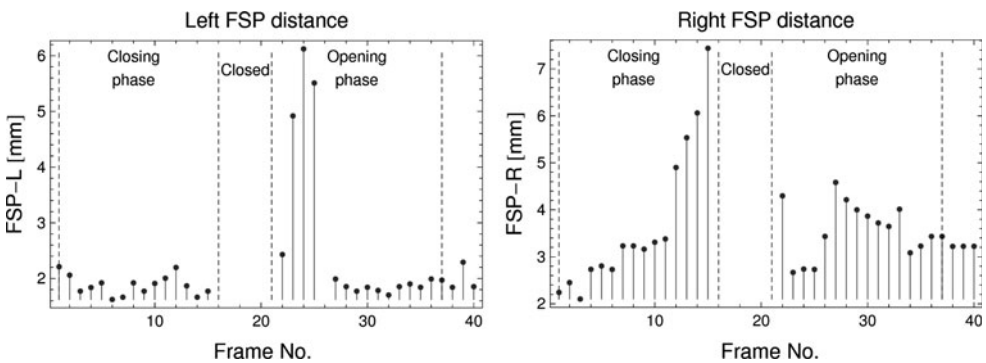


Fig. 15 Measurement 012v ($Re = 5{,}400$, with glottal closure), one oscillation cycle. Distance of the *left* and *right* flow separation point from the vocal fold apex

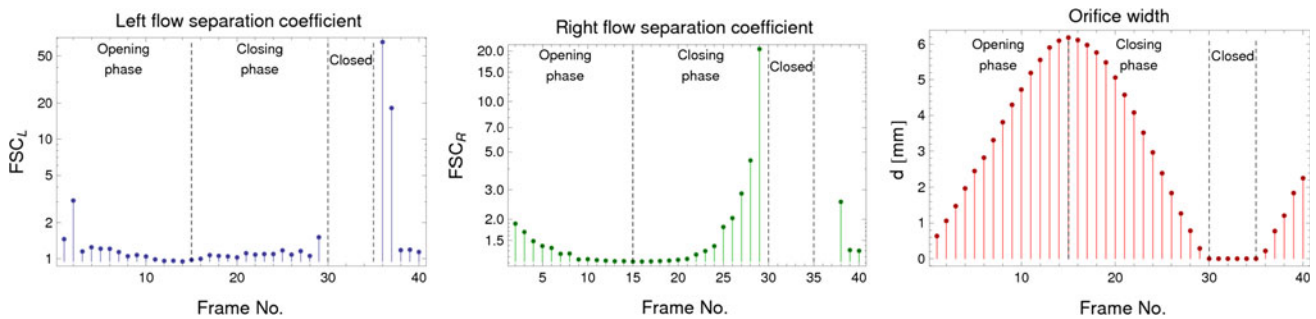


Fig. 16 Measurement 017c ($Re = 6{,}600$, with glottal closure), one oscillation cycle. *Left* and *right* flow separation coefficient, orifice width

separation locations measured using the model with a curved shape can have certain relevance to the other cases of phonation, too.

It should be also noted that the flow rates in the model are rather high relative to values known from human phonation and the duration of the phase when the vocal folds are closed (which is usually quantified by the *closed quotient*, CQ) lies in the lower bound of values encountered during loud speech. Nevertheless, the experience from other self-oscillating physical models (Pelorson et al. 1994; Thomson et al. 2005; Becker et al. 2009) shows that it is difficult to design a system behaving identically to the real vocal larynx, and even using approximate physical models, important and relevant results can be obtained.

The physical model was equipped with accelerometers monitoring vocal fold vibration. To measure the dynamic pressures and acoustic signals in the sub- and supraglottal spaces, pressure transducers and microphones were mounted in the setup. A PIV system synchronized with the vocal fold vibration was used to visualize the supraglottal airflow and to evaluate the position of the flow separation points along the vocal fold surfaces during their vibration. The airflow in the glottis can be to first approximation considered as two-dimensional: one may assume that the flow velocity does not change significantly along the length of the vocal folds (i.e., along the anterior–posterior axis z, see Fig. 2) in the very proximity of the glottis. This is not true further downstream, where turbulent structures dominate the flow field. The vorticity, aligned originally along the z-axis, interacts with the velocity field and creates inevitably a 3D velocity field. But when focused on the flow separation from the vocal fold surface, it is possible to draw meaningful data from PIV measurements in the coronal (x–y) plane.

In simplified glottal flow models based on Bernoulli or Euler equations where flow separation is taken into account, the position of the flow separation point is commonly considered as constant with respect to the narrowest cross-section. This implicitly assumes that the airflow is symmetric and separates at the same location from the left and right vocal fold. In current work, a modified criterion for flow separation (left and right flow separation coefficient—FSC), generalizing the classical criterion, was proposed. The results suggest that the usage of the classical flow separation criterion with constant values ranging between 1.1 and 1.5 is quite plausible, at least for the part of the oscillation cycle where the vocal folds are not too close together. Shortly before and after glottis closure, however, the aerodynamic effects are apparently much more complex and the criterion does not hold any more. The measured values of FSC demonstrate a general trend: shortly prior to and after glottal closure, either of the coefficients sharply increases, i.e., the glottal jet separates much further downstream of the narrowest cross-section. This is consistent with the qualitative results of Neubauer et al. (2007), who observed that during glottis opening, the jet is attached to the VF wall and strongly curved.

In a perfectly symmetrical glottal channel, the supraglottal flow field is bistable: the glottal jet does not remain symmetric, but tends to attach to either side of the channel. In the experiments, one of the directions was always preferential, although not exclusively. It seems that this was caused by minor asymmetries of the geometry, rather than by the fact that one of the model vocal folds was static. The same behavior was observed in the study of Erath and Plesniak (2010), who showed that even minor geometric irregularities cause the jet to skew to one of the directions with a high probability.

The physiological analogy to the current experimental setup would be unilateral vocal fold paralysis. The fact that one of the vocal folds in the model does not vibrate limits to certain extent the applicability of the results to real phonation. The current study is focused primarily on glottal aerodynamics and specifically dynamics of the glottal jet, which should not be largely different from the situation in the real larynx. Moreover, there have been even more dissimilar arrangements successfully used in experimental studies with synthetic and excised larynges, e.g., the hemilarynx configuration (one vocal fold colliding against symmetry plane). As long as a physical model representing all the important qualities of the real human larynx at once is not available, it is worth using approximative models that inevitably differ from reality in certain aspects.

The techniques used in this study for determining the location of flow separation were relatively laborious and time-consuming and required perfect adjustment of the experimental setup, in particular clean and well-focused optics. As some of the measurements did not provide sufficient contrast and resolution, only three measurements were evaluated. Even though these do not represent a comprehensive statistical data set, the authors believe that the results provide important new quantitative information, which cannot be found in the current literature.

In subsequent studies, several construction details and measurement techniques could be further improved. The state-of-the-art of the current PIV laser and camera systems, for instance, would allow a time-resolved measurement.

The current experimental setup does not contain a model of ventricular folds. It can be speculated what the influence of the ventricular folds on the position of the flow separation point is: depending on their distance from the vocal folds, they might both straighten the glottal flow axially or make it skew laterally even more. The authors believe it is a good starting point to obtain experimental data not biased by the presence of the ventricular folds. However, in the

future, it would be appropriate to perform a parametric study with various ventricular fold shapes and locations and determine their effect on supraglottal aerodynamics. With these modifications, the experimental setup could provide even more systematic and precise data on airflow separation and help to enlighten some of the fundamental aspects of human phonation.

Acknowledgments The research has been financially supported by the Grant Agency of the Academy of Sciences of the Czech Republic, project KJB200760801 *Mathematical modeling and experimental investigation of fluid–structure interaction in human vocal folds*, research plan AV0Z20760514. The support of ENSTA ParisTech, who provided the experimental background, is also gratefully acknowledged.

References

Alipour F, Scherer RC (2004) Flow separation in a computational oscillating vocal fold model. J Acoust Soc Am 116(3):1710–1719

Alipour F, Scherer RC (2006) Characterizing glottal jet turbulence. J Acoust Soc Am 119(2):1063–1073

Alipour F, Fan C, Scherer RC (1996) A numerical simulation of laryngeal flow in a forced-oscillation glottal model. Comput Speech Lang 10:75–93

Barney A, Shadle C, Davies P (1999) Fluid flow in a dynamic mechanical model of the vocal folds and tract. i. measurements and theory. J Acoust Soc Am 105(1):444–455

Becker S, Kniesburges S, Müller S, Delgado A, Link G, Kaltenbacher M, Döllinger M (2009) Flow-structure-acoustic interaction in a human voice model. J Acoust Soc Am 125(3):1351–1361

Cisonni J, Hirtum AV, Pelorson X, Willems J (2008) Theoretical simulation and experimental validation of inverse quasi-one-dimensional steady and unsteady glottal flow models. J Acoust Soc Am 124(1):535–545

Decker G, Thomson S (2007) Computational simulations of vocal fold vibration: Bernoulli versus Navier-Stokes. J Voice 21(3):273–284

Deverge M, Pelorson X, Vilain C, Lagrée P, Chentouf F, Willems J, Hirschberg A (2003) Influence of collision on the flow through in-vitro rigid models of the vocal folds. J Acoust Soc Am 114 (6 Pt 1):3354–3362

Erath B, Plesniak M (2006) The occurrence of the Coanda effect in pulsatile flow through static models of the human vocal folds. Exp Fluids 41:735–748

Erath B, Plesniak M (2006) The occurrence of the Coanda effect in pulsatile flow through static models of the human vocal folds. J Acoust Soc Am 120(2):1000–1011

Erath B, Plesniak M (2010) An investigation of asymmetric flow features in a scaled-up driven model of the human vocal folds. Exp Fluids. doi:10.1007/s00348-009-0809-0

Fox R, Kline S (1962) Flow regime data and design methods for curved subsonic diffusers. Trans ASME J Basic Eng 84:303–312

Hirtum AV, Pelorson X, Lagrée P (2005) In vitro validation of some flow assumptions for the prediction of the pressure distribution during obstructive sleep apnoea. Med Biol Eng Comput 43:162–171

Hofmans G, Groot G, Ranucci M, Graziani G, Hirschberg A (2003) Unsteady flow through in-vitro models of the glottis. J Acoust Soc Am 113(3):1658–1675

Horáček J, Šidlof P, Švec JG (2005) Numerical simulation of self-oscillations of human vocal folds with Hertz model of impact forces. J Fluids Struct 20(6):853–869

Krane M, Wei T (2006) Theoretical assessment of unsteady aerodynamic effects in phonation. J Acoust Soc Am 120(3): 1578–1588

Krane M, Barry M, Wei T (2007) Unsteady behavior of flow in a scaled-up vocal folds model. J Acoust Soc Am 122(6):3659–3670

Kucinschi B, Scherer R, Dewitt K, Ng T (2006) An experimental analysis of the pressures and flows within a driven mechanical model of phonation. J Acoust Soc Am 119(5 Pt 1):3011–3021

Li S, Scherer R, Wan M, Wang S, Wu H (2006) The effect of glottal angle on intraglottal pressure. J Acoust Soc Am 119(1):539–548

Lucero J (1998) Optimal glottal configuration for ease of phonation. J Voice 12(2):151–158

Neubauer J, Zhang Z, Miraghaie R, Berry D (2007) Coherent structures of the near field flow in a self-oscillating physical model of the vocal folds. J Acoust Soc Am 121(2):1102–1118

Pelorson X, Hirschberg A, van Hassel R, Wijnands A, Auregan Y (1994) Theoretical and experimental study of quasisteady-flow separation within the glottis during phonation. Application to a modified two-mass model. J Acoust Soc Am 96(6):3416–3431

Scherer R, Shinwari D, Witt KD, Zhang C, Kucinschi B, Afjeh A (2001) Intraglottal pressure profiles for a symmetric and oblique glottis with a divergence angle of 10 degrees. J Acoust Soc Am 109(4):1616–1630

Scherer RC, Shinwari D, Witt KJD, Zhang C, Kucinschi BR, Afjeh AA (2002) Intraglottal pressure distributions for a symmetric and oblique glottis with a uniform duct. J Acoust Soc Am 112(4):1253–1256

Sciamarella D, Quéré PL (2008) Solving for unsteady airflow in a glottal model with immersed moving boundaries. Eur J Mech B Fluids 27:42–53

Shinwari D, Scherer R, Dewitt K, Afjeh A (2003) Flow visualization and pressure distributions in a model of the glottis with a symmetric and oblique divergent angle of 10 degrees. J Acoust Soc Am 113(1):487–497

Šidlof P, Švec JG, Horáček J, Veselý J, Klepáček I, Havlík R (2008) Geometry of human vocal folds and glottal channel for mathematical and biomechanical modeling of voice production. J Biomech 41(5):985–995

Story B, Titze I (1995) Voice simulation with a body-cover model of the vocal folds. J Acoust Soc Am 97(2):1249–1260

Suh J, Frankel S (2007) Numerical simulation of turbulence transition and sound radiation for flow through a rigid glottal model. J Acoust Soc Am 121(6):3728–3739

Tao C, Zhang Y, Hottinger D, Jiang J (2007) Asymmetric airflow and vibration induced by the Coanda effect in a symmetric model of the vocal folds. J Acoust Soc Am 122(4):2270–2278

Thomson S, Mongeau L, Frankel S (2005) Aerodynamic transfer of energy to the vocal folds. J Acoust Soc Am 118(3 Pt 1): 1689–1700

Triep M, Brücker C (2010) Three-dimensional nature of the glottal jet. J Acoust Soc Am 127(3):1537–1547. doi:10.1121/1.3299202

Triep M, Brücker C, Schröder W (2005) High-speed PIV measurements of the flow downstream of a dynamic mechanical model of the human vocal folds. Exp Fluids 39:232–245

Vilain C, Pelorson X, Fraysse C, Deverge M, Hirschberg A, Willems J (2004) Experimental validation of a quasi-steady theory for the flow through the glottis. J Sound Vib 276:475–490

Zanartu M, Mongeau L, Wodicka G (2007) Influence of acoustic loading on an effective single mass model of the vocal folds. J Acoust Soc Am 121(2):1119–1129

Zhang Z (2008) Influence of flow separation location on phonation onset. J Acoust Soc Am 124(3):1689–1694. doi:10.1121/1.2957938

Zhang Z, Neubauer J, Berry D (2007) Physical mechanisms of phonation onset: a linear stability analysis of an aeroelastic continuum model of phonation. J Acoust Soc Am 122(4): 2279–2295